Available online at www.sciencedirect.com
ScienceDirect
Advances in Space Research 42 (2008) 181–191
ADVANCES IN SPACE RESEARCH (a COSPAR publication)
www.elsevier.com/locate/asr

Magnetospheric electric field variations caused by storm-time shock fronts

M. Kokorowski [a,*], E.A. Bering III [b], M. Ruohoniemi [c], J.G. Sample [d], R.H. Holzworth [a], S.D. Bale [d], J.B. Blake [e], A.B. Collier [f], A.R.W. Hughes [f], E.H. Lay [a], R.P. Lin [d], M.P. McCarthy [a], R.M. Millan [g], H. Moraal [h], T.P. O'Brien [e], G.K. Parks [d], M. Pulupa [d], B.D. Reddell [b], D.M. Smith [i], P.H. Stoker [h], L. Woodger [g]

[a] *University of Washington, Department of Earth and Space Sciences, Seattle, WA 98195, USA*
[b] *Physics Department, University of Houston, 617 Science and Research I, Houston, TX 77204-5005, USA*
[c] *Applied Physics Laboratory, Johns Hopkins University, 11100 Johns Hopkins Road, Laurel, MD 20723-6099, USA*
[d] *University of California at Berkeley, Space Sciences Laboratory, Berkeley, CA 93923, USA*
[e] *Aerospace Corporation, Box 92957, Los Angeles, CA 90009-2957, USA*
[f] *University of KwaZulu-Natal, Physics Department, Durban 4001, South Africa*
[g] *Dartmouth College, Department of Physics and Astronomy, Hanover, NH 03755, USA*
[h] *North-West University, School of Physics, Potchefstroom 2520, South Africa*
[i] *University of California at Santa Cruz, SCIPP, Santa Cruz, CA 95064, USA*

Received 9 November 2006; received in revised form 7 March 2008; accepted 11 March 2008

Abstract

On January 20, 2005 there was an X 7.1 solar flare at 0636 UT with an accompanied halo coronal mass ejection (CME). The resultant interplanetary shock impacted earth ~36 h later. Near earth, the Advanced Composition Explorer (ACE) spacecraft observed two impulses with a staircase structure in density and pressure. The estimated earth-arrival times of these impulses were 1713 UT and 1845 UT on January 21, 2005. Three MINIature Spectrometer (MINIS) balloons were aloft on January 21st; one in the northern polar stratosphere and two in the southern polar stratosphere. MeV relativistic electron precipitation (REP) observed by all three balloons is coincident (<3 min) with the impulse arrivals and magnetospheric compression observed by both GOES 10 and 12. Balloon electric field data from the southern hemisphere show no signs of the impulse electric field directly reaching the ionosphere. Enhancement of the balloon-observed convection electric field by as much as 40 mV/m in less than 20 min during this time period is consistent with typical substorm growth. Precipitation-induced ionospheric conductivity enhancements are suggested to be (a) the result of both shock arrival and substorm activity and (b) the cause of rapid (<6 min) decreases in the observed electric field (by as much as 40 mV/m). There is poor agreement between peak cross polar cap potential in the northern hemisphere calculated from Super Dual Auroral Radar Network (SuperDARN) echoes and horizontal electric field at the MINIS balloon locations in the southern hemisphere. Possible reasons for this poor agreement include (a) a true lack of north–south conjugacy between measurement sites, (b) an invalid comparison between global (SuperDARN radar) and local (MINIS balloon) measurements and/or (c) radar absorption resulting from precipitation-induced D-region ionosphere density enhancements.

Keywords: Electric field; Convection; Substorm; Relativistic electron precipitation; Shock wave

1. Introduction

Observations of interplanetary shocks that impinge upon the magnetosphere are relatively new with the first well-studied case occurring on March 24, 1991 (e.g. Mullen

* Corresponding author. Tel.: +1 206 543 4914.
E-mail address: mkoko@u.washington.edu (M. Kokorowski).

0273-1177/$34.00 © 2008 COSPAR. Published by Elsevier Ltd. All rights reserved.
doi:10.1016/j.asr.2008.03.006

et al., 1991; Vampola and Korth, 1992; Blake et al., 1992; Wygant et al., 1994). Electromagnetic fields associated with interplanetary shocks can be responsible for energizing seed particle populations creating new radiation belts (Li et al., 1993; Hudson et al., 1995, 1997; Elkington et al., 2002). These radiation belts can last for months to years, which has forced a re-evaluation of radiation belt formation mechanisms. Strong electric fields within the magnetosphere can also provide either the transport or change in pitch angle necessary to cause radiation belt electrons to precipitate into the earth's atmosphere. According to Gosling et al. (1990) storm sudden commencement (SSC) compression of the magnetosphere by interplanetary shocks is generally caused by coronal mass ejections (CMEs). At 0636 UT on January 20, 2005, a CME was emitted from the sun, which resulted in a two-step shock that was observed by the ACE satellite at 220 earth radii sunward of earth at 1642 UT on January 21, 2005. Fig. 1 shows the solar wind dynamic pressure and the z-component of the interplanetary magnetic field (IMF B_z) as measured by ACE with the data time shifted to subsolar earth geosynchronous. The earth-arrival times of this two-step shock are 1713 UT and 1845 UT on January 21. According to GOES magnetometer data and output from two magnetopause models (Petrinec and Russell, 1996; Shue et al., 1997, 1998), the second step of the shock compressed the dayside magnetopause to within geosynchronous orbit (see Figs. 2 and 3).

The first well-documented case of the interplanetary shock electric field effects on the magnetosphere were observed by the Combined Release and Radiation Effects Satellite (CRRES). On March 24, 1991, CRRES successfully witnessed the formation of new electron and proton radiation belts (Vampola and Korth, 1992; Blake et al., 1992). The formation of these radiation belts was attributed to the energization of the seed particles by resonance interaction of the electron drift motion with the time-varying electric field. Electrons with energies greater than 6 MeV and protons with energies >20 MeV were deposited near $L = 2.5$. The interplanetary shock-induced electric and magnetic field amplitudes were measured by CRRES and the subsequent sinusoidal variations in electron particle flux modulated by the shock were key features modeled both analytically and computationally. Li et al. (1993) created an analytical model that successfully duplicated the azimuthal propagation of the initial pulse of the shock. Additional information such as the propagation speed and spatial size of the shock front were derived from this model. Hudson et al. (1995, 1997) successfully tracked the proton flux as it was responding to the decaying oscillating electric field. Test particle simulations in MHD fields of proton (Hudson et al., 1997) and electron (Elkington et al., 2002) transport were conducted with assumed interplanetary shock arrival conditions (no upstream solar wind measurements were available for the March 1991 event). The newly created radiation belts from this event existed for months (protons measured by CRRES) to years (electrons measured by SAMPEX, Looper et al., 1994). Stably trapped energetic particles pose problems for vulnerable spacecraft that must pass through the radiation belts.

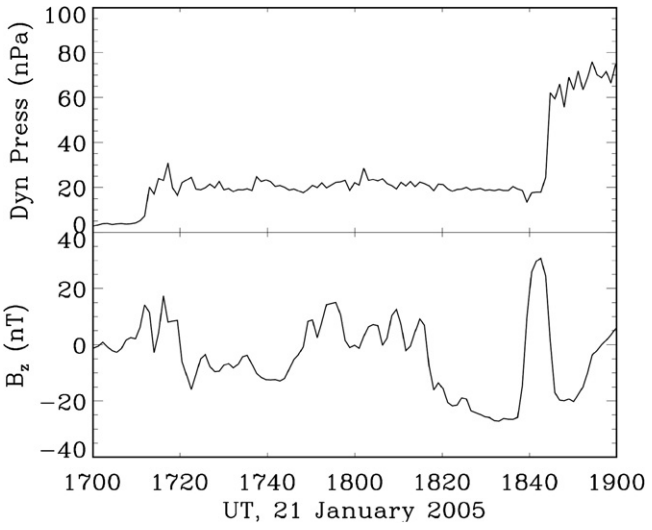

Fig. 1. IMF B_z and solar wind dynamic pressure measured by the ACE spacecraft on January 21, 2005 time shifted to earth geosynchronous orbit. The two-step impulses are visible at 1713 UT and 1845 UT.

The MINIature Spectrometer (MINIS) project was designed to observe relativistic electron precipitation (REP) phenomena. The primary purpose of the MINIS balloon campaign was to measure bremsstrahlung X-rays created from precipitating MeV radiation belt electrons and any associated stratospheric electric and magnetic fields at multiple locations. Initial results relating the electric field response to the CME-induced solar energetic proton (SEP) event on January 20, 2005 are presented by Kokorowski et al. (2006). X-ray observations during the January 21, 2005 REP events are presented by Sample et al. (submitted for publication). Fortuitously, two MINIS balloon payloads with electric field instrumentation were aloft in the stratosphere (~32 km) on January 21, 2005 during the interplanetary shock arrival and several REP events. Only the four payloads launched from the southern hemisphere had electric field instrumentation. Between 1710 UT and 2000 UT, while in the afternoon-dusk MLT sector, MINIS flights 2S and 3S observed two separate simultaneous REP X-ray bremsstrahlung events. Large amplitude horizontal electric fields (up to 60 mV/m) were detected during this same period.

In this paper, we examine the effects of the two-step impulse on the coupled magnetosphere–ionosphere system from an electric field perspective. Specifically, we suggest that large amplitude electric fluctuations observed by both MINIS 2S and 3S are a consistent with typical substorm growth combined with sudden precipitation-induced ionospheric conductivity enhancements. We determine that the relatively simple analytical model of Li et al. (1993), which characterizes shock impulse propagation, cannot be easily compared directly to MINIS electric field measurements.

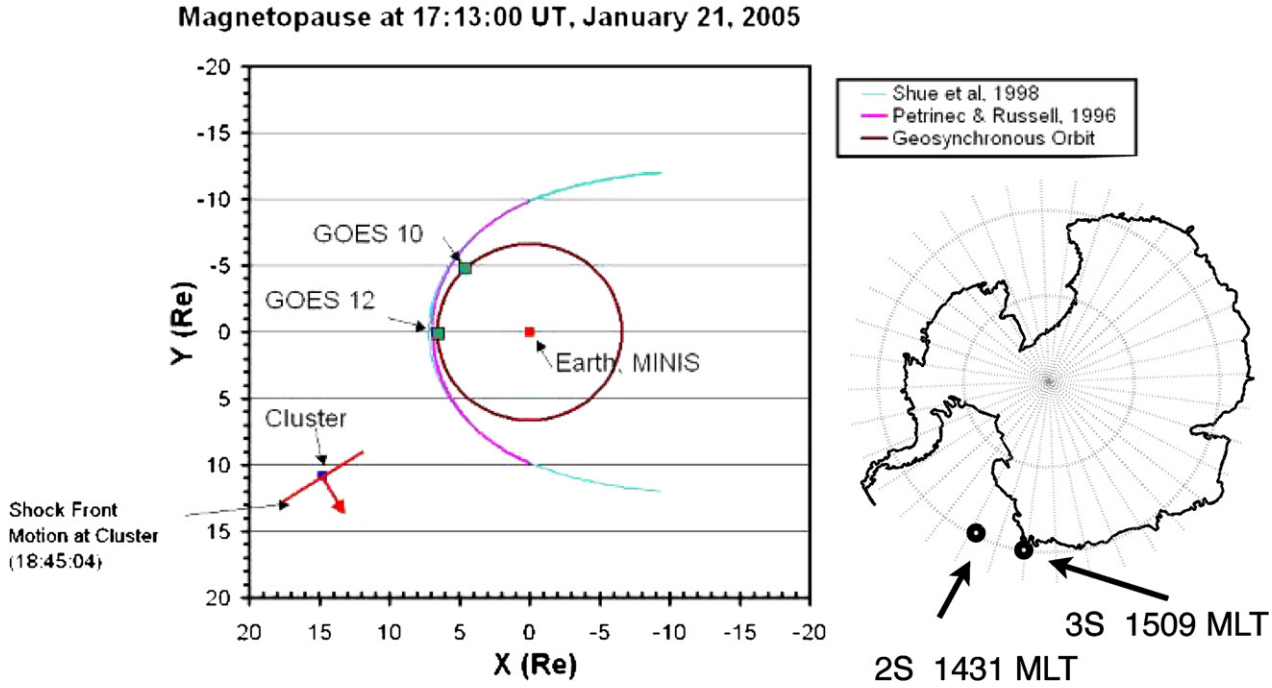

Fig. 2. Near-earth magnetosphere configuration at 1713 UT on January 21, 2005 and zoom on MINIS balloon locations above Antarctica. The magnetosphere view is looking in the $-Z_{GSE}$ direction. Models show the magnetopause crossing near geosynchronous orbit at this time. The normal direction of the second step of the shock at Cluster is shown. MINIS 2S and 3S MLT locations are shown looking from the north through the earth in the same coordinates as the magnetosphere view. MLT is based on IGRF/DGRF model output.

Lastly, we show that there is insufficient evidence in the combined Super Dual Auroral Radar Network (SuperDARN) and MINIS electric field data sets to extrapolate the local impulse effects at the MINIS balloons into the northern hemisphere.

2. MINIS instrumentation

In January 2005, the MINIS campaign provided the first opportunity for multi-point balloon-borne measurements of REP events up to MeV energies, including simultaneous observations at different longitudes and at near-conjugate locations. The primary instrument on each balloon was a sodium iodide X-ray spectrometer for measuring the bremsstrahlung produced by REP. In this paper, we present X-ray counts recorded into four broad energy channels (20–175, 175–540, 540–825, and 825–1500 keV) at 20 Hz. Two balloons were launched from Churchill, Manitoba, Canada at 0850 UT on January 21 and 0140 UT on January 25. Four balloons, each carrying an X-ray spectrometer, a z-axis search coil magnetometer, and a 3-axis electric field instrument providing dc-electric field and VLF measurements in three frequency bands, were launched from the South African National Antarctic Expedition (SANAE) IV. The southern launches took place at 1400 UT on January 17, 1309 UT on January 19, 2115 UT on January 20, and 0950 UT on January 24.

The main electric field instrumentation consisted of a set of three double Langmuir probes similar to those described by Holzworth and Bering (1998). In fair weather, away from thunderstorm activity, horizontal electric field at 32 km altitude is thought to be the 1 s, >100 km average of the overlying ionospheric electric field (Mozer and Serlin, 1969). Spherical probes of 15 cm diameter were placed away from the main balloon payloads. The probes were coated with a colloidal suspension of carbon (Aquadag) to provide a large, uniform surface work function, thereby suppressing photoemission of electrons and minimizing a source of dc offset. Four probes forming orthogonal axes in the horizontal plane were placed 2 m from the payload center. Two vertical probes where suspended on the balloon load line roughly 2 m and 3 m above the payload, respectively, and were rigidly separated from each other by 1 m. High-impedance electronics allowed for a direct measurement of the voltage between each sphere and the payload ground. The entire payload was rotated about the vertical axis with a period of roughly 40 s in order to identify any non-geophysical dc offsets in the horizontal measurements.

3. Observations

In this section, we first examine satellite data from Cluster and GOES in order to see when the interplanetary shock arrived at earth and that, as a result of their arrival, the magnetopause moved to within geosynchronous orbit. Then, we present some MINIS balloon observations of both particles and electric field, which we relate to the

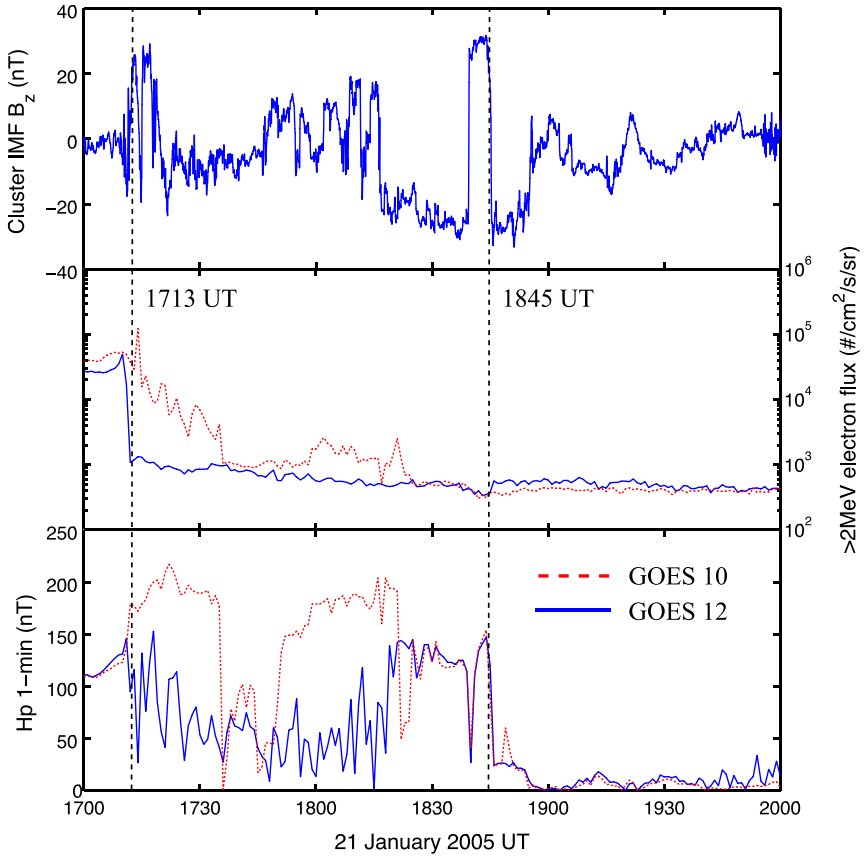

Fig. 3. The top panel shows Cluster observations of IMF B_z (nT). The middle panel shows GOES 10 (dashed line) and GOES 12 (solid line) >2 MeV electron flux (#/cm^2/s/sr). The bottom panel shows GOES 10 (dashed line) and GOES 12 (solid line) parallel magnetic field (Hp in nT) for January 21, 2005. The two vertical dashed lines indicate the estimated arrival times for each impulse step at geosynchronous.

shock later in the following sections. Lastly, we introduce some SuperDARN radar observations of the northern polar ionosphere for comparison with MINIS electric field measurements in the southern hemisphere.

3.1. Satellite observations

Fig. 2 shows the configuration of the magnetopause at the arrival of the first interplanetary shock at 1713 UT on January 21, 2005. At this time the shock begins to compress the magnetosphere, pushing the dayside magnetopause to very near geosynchronous orbit. In Fig. 2, two magnetopause models were used to approximate the position of the dayside magnetopause at 1713 UT. Shue et al. (1998) and Petrinec and Russell (1996) produce very similar locations because both models are essentially empirical fits to the following formula

$$r = r_0\left(\frac{2}{1+\cos\theta}\right)^{\alpha}. \quad (1)$$

In Eq. (1), r is the radial distance of the magnetopause, θ is the solar zenith angle, and r_0 and α are parameters that depend on the IMF B_z and the dynamic pressure of the solar wind. Both models require IMF B_z and solar wind dynamic pressure as inputs. The ACE-measured IMF B_z of 18 nT and dynamic pressure of 23 nPa were used for the model inputs. In Fig. 2 at 1713 UT, GOES 10 and 12 satellites were located at 0800 and 1200 MLT, respectively.

Fig. 3 is presented to show the overall impulse compression of the magnetosphere at GOES 10 and 12 along with consistency between ACE and the near-earth Cluster magnetic field fluctuations. Fig. 3 shows Cluster IMF B_z (top panel) as well as >2 MeV electron flux (middle panel) and the parallel (to earth's rotation axis) component of the magnetic field (Hp, bottom panel) at both GOES 10 and GOES 12. From this figure, we see that solar wind IMF B_z at Cluster is very similar to what is seen at ACE. Both satellites observe more distinct magnetic field changes just before the second impulse at 1845 UT (time shifted for the ACE data to geosynchronous arrival). Several instances of prolonged southward magnetic field tell us that there is potential for substorm growth. We can also see how the magnetopause and the bow shock pass geosynchronous orbit at each GOES spacecraft. Upon arrival of the first impulse, at 1712 UT GOES 12 measured the beginning of energetic electron flux decrease from 5.0×10^4 to 1×10^3 particles/cm^2/s/sr in a matter of minutes. The electron flux decreases to 1×10^2 particles/cm^2/s/sr by the end of the day (by 2400 UT, not shown in Fig. 3). Likewise, beginning 2 min later (1714 UT) GOES 10 measured a similar

decrease in electron flux over the course of a 20-min interval. For each GOES satellite, the parallel magnetic field is near 110 nT inside the magnetosphere before the interplanetary shock arrives (Fig. 3, bottom panel, before 1712 UT) and eventually reaches a value of 10 nT in the solar wind (Fig. 3, after 1845 UT). As shown in Fig. 2, GOES 12 is closer to the subsolar point than GOES 10 and the two are separated by 4 h of local time. Consequently, there were significant differences in response. GOES 12 appears to enter the magnetosheath at 1713 UT and remains in the sheath region until 1845 UT. On the other hand, GOES 10 remained inside a compressed magnetosphere until 1736 UT, was in the sheath from 1736 UT to 1750 UT and then moved back inside the magnetosphere from 1750 UT to 1822 UT. After 1822 UT, both spacecraft are in similar regions. They appear to be in an intensified sheath from 1822 UT until 1845 UT and in the solar wind afterward.

3.2. MINIS balloon observations

On January 21, 2005, MINIS flight 2S was located at $L = 3.5$, flight 3S was positioned at $L = 4.1$ and they were separated by 38 min of MLT as calculated by the IGRF/DGRF model (see Fig. 2). Flights 2S and 3S observed intense periods of hard bremsstrahlung in the interval shown in Fig. 4 from 1700 to 2000 UT. The top two panels of Fig. 4 show the four-channel X-ray counts during this precipitation interval. We will break the precipitation down into two principal event periods: 1710–1740 UT and 1830–1915 UT. Each period contains one of the impulse arrivals marked with vertical dashed lines at 1713 UT and 1845 UT in Fig. 4. Precise onset timing of the first period is difficult because of small data gaps in the Iridium telemetry. However, even with these gaps, onset of this burst of precipitation observed by MINIS 2S and 3S is within 3 min. This first event was seen most strongly on MINIS 3S, and the spectral shape at the two southern payloads, separated by 660 km, is similar to a few percent in a power-law fit from 150 to 600 keV (see Sample et al., submitted for publication, for more detail). The events lasted ~30 min, which is similar to previous events seen by INTERBOA (International Balloon Observations of Aurora) (Foat et al., 1998) and MAXIS (MeV Auroral X-ray Imaging Spectrometer) (Millan et al., 2002).

From 1833 to 1845 UT only flight 3S, the higher L shell southern balloon, observes precipitation. However, at 1845 UT flight 2S and 3S were separated by 660 km when they observed a near-simultaneous precipitation event which began in the more westerly 2S only 3 s before 3S. As discussed more completely in Sample et al. (submitted for publication), this event is not consistent with an eastward drifting patch of precipitation. Similar intensities and nearly identical spectra are observed at both payloads from 1845 to 1905 UT. Interestingly, both of the near-simultaneous REP burst observations are coincident (to within minutes) of large, rapid increases in the Sym-H index of more than 40 nT in less than 3 min in each case (see the bottom panel of Fig. 4). This Sym-H increase is indicative of the magnetospheric compression expected to result from an interplanetary shock.

The horizontal electric fields for flights 2S and 3S are also shown in Fig. 4 in the third and fourth panels. These curves represent 1-min sliding average data advanced 30 s per point in earth-fixed local geomagnetic coordinates. MINIS 3S was poleward of MINIS 2S ($L = 4.1$ as opposed to $L = 3.5$) and later in local time (by 38 min). During the first precipitation event, which is roughly coincident with the arrival of the first shock impulse at 1713 UT (to within 3 min), the horizontal electric field components remain relatively unperturbed with magnitudes below 10 mV/m. There are no apparent immediate electric field responses to this first impulse at either balloon location. After the first impulse, both balloons observed relatively gradual and modest (in amplitude) horizontal electric field fluctuations. More distinct similarities between the two balloons can be seen beginning at about 1822 UT. Both balloons observe a significant enhancement in the electric field, predominately in the pole ward component. This amplitude growth follows a distinct and persistent southward IMF seen at ACE and Cluster by about 8 min. The local maxima at 2S and 3S do not occur at exactly the same time. Each balloon also observes a rapid (<3 min) decrease in electric field amplitude. For each balloon, this is coincident with the onset of local REP. In the case of 2S, this rapid electric field decrease and locally observed REP is coincident with the second impulse at 1845 UT. At 3S, both the electric field decrease and REP preceded the second shock impulse by 12 min.

3.2.1. MINIS-derived ionospheric convection

Fig. 5 shows the ionospheric convection pattern derived from the MINIS 2S and 3S electric field measurements. The clockdial image is a plot of the South Pole as viewed from above. The plasma drift velocity vectors were computed from the MINIS-observed electric and magnetic field measurements with the following equation

$$V_D = \frac{E \times B}{B^2}. \quad (2)$$

Plasma velocity vectors are plotted as a function of magnetic local time (outer circle) and universal time (inner circle). Vector tails are fixed onto the circles and the heads point in the plasma flow direction. Flight 2S convection vectors are plotted on the outer ring and 3S vectors are on the inner ring. Following 1400 MLT and lasting for several hours, both balloons see bursts of convection, with flow velocities greater than 1000 m/s. Between 1730 and 1900 UT, strong convection flows are predominately sunward (westward).

3.3. SuperDARN observations

During the UT evening of January 21, 2005, northern hemisphere SuperDARN radar measurements were avail-

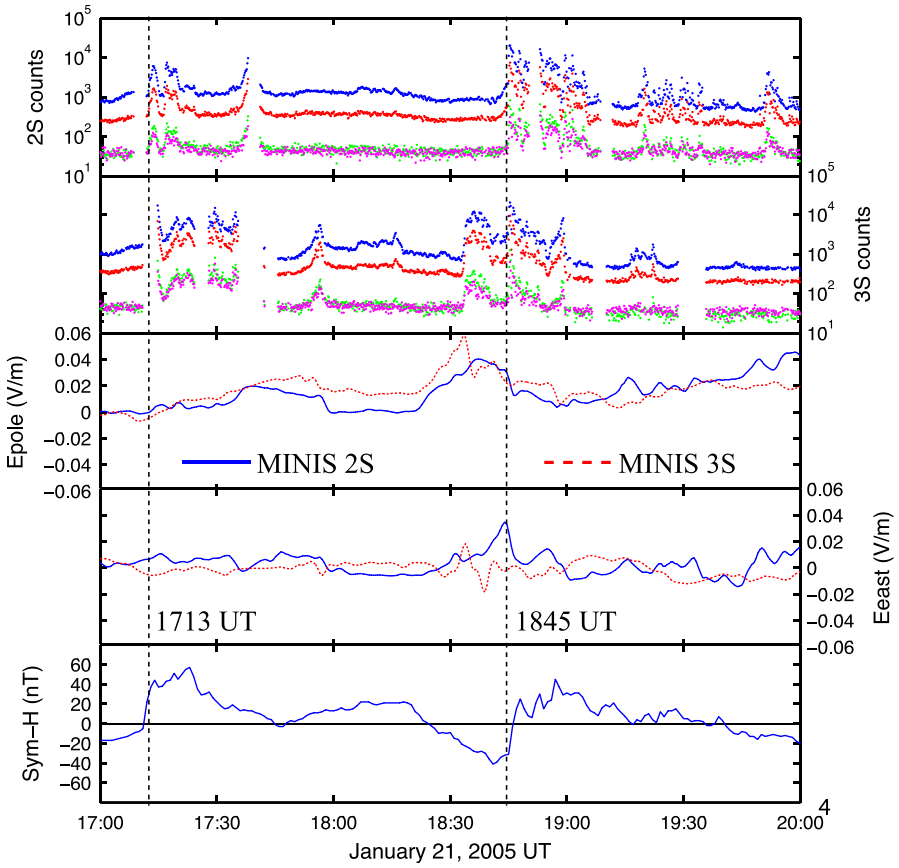

Fig. 4. The top two panels show MINIS 2S and 3S total X-ray counts from 1700 to 2000 UT on January 21, 2005. Four energy channels are plotted, 0–175 keV, 175–540 keV, 540–825 keV, and 825–1500 keV. The next two panels show the MINIS 2S and 3S eastward and poleward horizontal electric fields. The bottom panel is Sym-H magnetic index courtesy of the Kyoto World Data Center. The arrival of the two-step shock is marked by vertical dashed lines at 1713 UT and 1845 UT.

able for comparisons with the MINIS balloon horizontal electric field data. SuperDARN data and convection map model output from northern hemisphere sites are shown in Fig. 6 along with the same MINIS 2S and 3S electric field data as in Fig. 4. Fig. 6 compares the times of peak northern hemisphere SuperDARN cross polar cap potential (CPCP) with the times of peak electric fields observed by the southern hemisphere balloons. In the SuperDARN plots, the location of the balloon conjugate point moves from ~1430 MLT to ~1630 MLT at ~57° MLAT for the entire interval. The conjugate points to both balloons were within the field of view of one of the SuperDARN radars (Goose Bay). This means that the radar array is capable of observing echoes in the northern hemisphere ionosphere that are magnetically conjugate to the ionosphere above the MINIS balloons. However, there are only a few total echoes and none above MINIS-conjugate locations. This makes direct data comparison impossible. Without a direct data comparison, we can still compare the modeled convection maps with the MINIS observations.

In Fig. 6, we focus on the SuperDARN CPCP and the MINIS poleward horizontal electric field relative to impulse arrival times. Minutes after the impulse at 1713 UT, the peak inferred northern CPCP was 57 kV and occurred at 1722 UT. There was no significant electric field change at the MINIS 2S and 3S locations at that time. More than 35 min prior to the second, more pronounced impulse arrival at 1845 UT, SuperDARN radars inferred a peak CPCP of 77 kV at 1806 UT. The peak MINIS balloon-measured electric field occurred at 1838 UT and 1832 UT for 2S and 3S, respectively.

4. Discussion

We have established a timeline for satellite, balloon and radar observations during the impulse period between 1700 UT and 2000 UT on January 21, 2005. We can follow the interplanetary shock arrival from ACE (Fig. 1), the response of the magnetosphere in the form of a moving magnetopause from GOES 10 and 12 (Figs. 2 and 3) and relativistic electron precipitation and electric field fluctuation at both southern MINIS balloons (Fig. 4). In this section, we relate the observed electric field measurements to the shock impulse arrival and solar wind IMF conditions. We compare the whole of the presented observations to typical substorm development. Finally, MINIS electric field convection measurements in the southern hemisphere

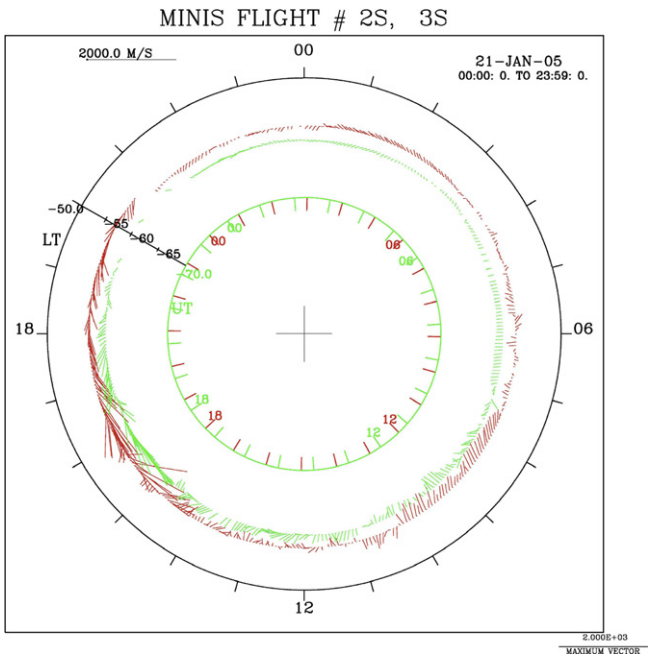

Fig. 5. Clockdial plot for January 21, 2005. The outer ring is MINIS 3S convection velocity vectors and inner ring are the MINIS 2S convection vectors. Local time is give on the outside dial and universal time is given on the inside dial.

are compared with northern hemisphere SuperDARN radar observations and convection maps.

4.1. Electric field response

GOES 10, 12, Cluster and MINIS 2S, 3S all observe near-simultaneous fluctuations in electron flux and/or magnetic field at 1713 UT due to the first interplanetary shock arrival over a range of MLT values and L shells. The drop in GOES electron flux along with the magnetic impulse observed by Cluster and ACE suggest that REP measurements at MINIS 2S and 3S are directly linked to a magnetospheric compression (see Clilverd et al., 2007 for more REP observations and discussion). However, did the MINIS balloons directly observe the shock impulse electric field? According to Araki et al. (1997) the magnetic field impulse during the March 24, 1991 SSC event traveled from geosynchronous to the ionosphere within a minute. Since the MINIS balloons did not measure any rapid electric field fluctuations within minutes of the first impulse, it could be that the impulse never reached the balloons at all. However, if the January 21, 2005 impulse were short in duration (~1 min), as was stated by Li et al. (1993) for the March 24, 1991 event, then any signature that the MINIS balloons could possibly observe might be missed by numerous small data gaps. One-second sampled data were examined to insure 1-min averaging did not wash out any signature. There is no evidence in the raw electric field data (not shown) for any rapid impulse fluctuation. With that said, we cannot completely rule out that an impulse reached the balloon locations and was missed.

We show that the slow electric field variations observed by both MINIS balloons are consistent with expected substorm growth following a period of southward IMF despite uncertainty in the impulse propagation. Dayside reconnection, based on Dungey (1961), will drive convection in the magnetosphere without any SSC. Enhanced convection electric fields observed by polar stratospheric balloons can be a direct result of a typical southward IMF B_z induced substorm (Mozer and Serlin, 1969). However, there is an average delay of 15 min between the time when the IMF turns southward and when the convection becomes enhanced (McPherron, 1970). Looking at the IMF B_z measured by ACE (Fig. 1), we can see two distinct periods of southward IMF starting at 1720 UT and 1815 UT. Then, looking at Fig. 4, we can see that MINIS 2S and 3S both observe poleward electric field enhancements consistent with increased plasma convection on the order of 15 min after each time the IMF turns southward. Thus, we conclude that both MINIS payloads observed REP events are likely to be directly linked to each impulse event and that the poleward electric field intensifications are consistent with typical substorm growth. What about the decreases observed in the electric field?

As seen in Fig. 4, there are several instances of rapid electric field decreases observed at 1833 UT by flight 3S and 1845 UT by flight 2S. In each case, both components of the electric field decrease by at least a factor of two in less than 3 min. Additionally, both instances are accompanied by precipitation enhancements at each individual location. Energetic particles, including visible auroral electrons, relativistic electrons and incident solar energetic protons, collide with atmospheric neutrals as they precipitate. These collisions ionize a fraction of the neutrals and increase the local conductivity. Increased ionospheric/atmospheric ionization caused by energetic particle precipitation has been proposed by Mozer et al. (1973), modeled by Coumans et al. (2004) and Seppälä et al. (2004) and observed by Bering et al. (1991) and Kokorowski et al. (2006). The exact ionospheric conductivity enhancement for this particular event has not, at present, been modeled and was not measured directly above the balloon payloads. Even without explicit modeling, we know that there is precipitation from relativistic electrons and energetic protons from the largest ground level enhancement since 1956 on the previous day at 0655 UT (Bieber et al., 2005). Energetic proton flux (>1 MeV) increased by over an order of magnitude at GOES 11 on January 20, 2005 (see Kokorowski et al., 2006, Fig. 1) and had not yet returned to background levels by 1700 UT the following day on 21 January 2005 (not shown). In order to affect conductivity at the stratospheric balloon altitude, the incident particle energy must be much greater than typical aurora or even several MeV REP electrons. Thus, looking for a conductivity enhancement at either MINIS balloon on January 21st may not be meaningful considering the flux of energetic protons which can reach balloon altitudes (>100 MeV) had reduced to near background levels. However, if we assume a constant ion-

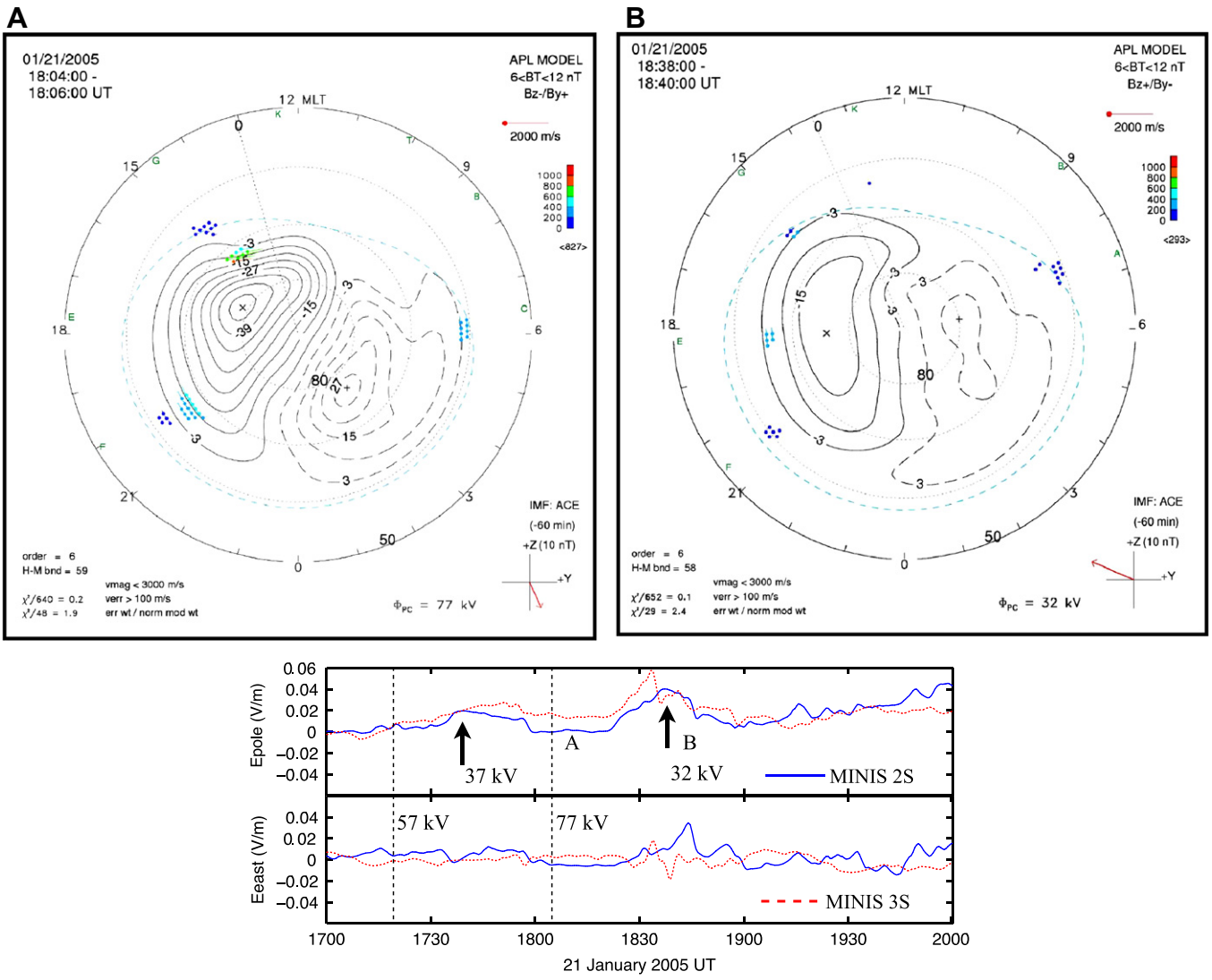

Fig. 6. Correlation between SuperDARN northern hemisphere peak convection with MINIS 2S and 3S 1 min averaged horizontal electric fields as in Fig. 4. Two representative SuperDARN convection maps are shown for 1804 UT and 1836 UT. The two vertical dashed lines are the temporal SuperDARN cross cap potential maximums. The two arrows highlight the MINIS 2S observed electric field maximums. At each of the two times where MINIS 2S is at a local maximum, the SuperDARN cross cap potential is given.

ospheric current density, and that Ohm's law ($j = \sigma E$) applies, a factor of two increase in the ionospheric conductivity due to the effects of precipitation above the MINIS balloon payload could explain the factor of two decrease in the observed electric field. This would explain the two rapid electric field decreases seen at 1833 UT and 1845 UT seen at MINIS 3S and 2S, respectively. According to Coumans et al. (2004), a factor of two ionospheric conductance increase is within reason for a nominal substorm. De la Beaujardiere et al. (1981) describe how the an auroral arc conductivity increase can lead to either a measured electric field increase or a decrease based on the configuration of polarization electric field within auroral arc itself. In this case, with energetic particle precipitation, we have supposed that either an anti-correlation or asymmetric type polarization electric field configuration (as discussed in De la Beaujardiere et al., 1981) is present. Both of these would cause the observed electric field decrease. More work confirming the geometry of the precipitation region and modeling the conductivity enhancement is needed to solidify this assumption. However, we propose that both impulse-driven (2S at 1845 UT) and substorm-related (3S at 1833 UT) REP conductivity enhancements caused a drop in the local ionospheric electric field.

In order to learn more about how the impulse events on January 21, 2005 connect to the MINIS electric field and REP observations, applying analytical and computational models would be useful. However, since the relatively simple Li et al. (1993) model is restricted to the equatorial plane, it is not clear how well the model maps to the ionosphere for comparison with the MINIS observations at $L > 3.5$. Additionally, small MINIS data gaps create fur-

ther uncertainty that an impulse could have propagated to the balloon at all. In order to properly characterize the entire magnetosphere during this shock event and compare to MINIS observations, more complete numerical models must be employed like those of Hudson et al. (1995, 1997) and Elkington et al. (2002). A full numerical treatment of this event is beyond the scope of this paper.

4.2. Poor agreement between superDARN and MINIS

In order to gain insight into the global response of the polar ionosphere in both the northern and southern hemispheres, we compare electric field fluctuations between SuperDARN measurements and MINIS observations. As mentioned in Section 3.3, we cannot make a direct data comparison between SuperDARN echoes and the MINIS-observed horizontal electric field. However, we can look for signs of conjugacy between the northern hemisphere convection map model output and MINIS observations. For the SuperDARN convection maps, high frequency (HF) backscatter from the total radar array and interplanetary magnetic field information are used as input to a statistical model, which outputs convection patterns from which the cross polar cap potential (CPCP) is determined (Ruohoniemi and Baker, 1998). MINIS electric field measurements, on the other hand, are local observations of the large-scale ionospheric electric field directly above the balloon. If we were able to see a temporal correlation between conjugate electric field behavior, we could then extrapolate our local electric field onto larger, perhaps global scales. However, there is insufficient evidence to claim that we could extend local MINIS observations into the northern hemisphere. Below, we will briefly summarize the SuperDARN and MINIS observations and then propose physical reasons why there is poor agreement between the two.

The best example of a poor agreement between the SuperDARN convection model output and the MINIS observations can been seen in Fig. 6 near the second impulse time at 1845 UT. Both MINIS 2S and 3S observe relatively large horizontal electric fields before rapid drops at the arrival time (1845 UT, 2S) and minutes prior to the arrival (1833 UT, 3S). However, from the SuperDARN convection maps, there is neither a CPCP maximum or a rapid decrease of the CPCP observed near the second impulse arrival. This is just one example that can be seen in Fig. 6 of the SuperDARN CPCP and MINIS local electric field maxima occurring at different times.

There are several factors that could help account for the lack of evidence for coincident maxima in SuperDARN CPCP and MINIS horizontal electric field. First of all, there could be a true difference in the northern and southern time-dependent CPCP. Although previous studies have shown that both polar caps have the same general characteristics during a given substorm or quiet time period (Bering and Benbrook, 1987), no global one-to-one connections have been made. Also, during January, we expect some conductivity asymmetries between the northern and southern polar cap simply due to the seasonal solar illumination. Second, a local electric field maximum observed by a single balloon does not directly imply a maximum in the CPCP. As is clear in Fig. 6, the local maxima observed by each MINIS balloon are not exactly coincident even if there are some general trends. Thus, while SuperDARN CPCPs and maximum balloon-observed potential differences are related, they are intrinsically different and cannot be compared one-to-one. The final consideration to take into account is energetic particle precipitation causing enhancements in plasma density and conductivity. SuperDARN radar echo depends on the presence of plasma irregularities and adequate F-region plasma density, both of which should have been present in abundance during this disturbed interval. However, the relatively small number of observed SuperDARN echoes suggests that there may have been significant D-region HF signal absorption. Loss of HF radar backscatter has been noted during substorms in the past (Gauld et al., 2002; Yeoman et al., 1997) and has been directly attributed to absorption in and enhanced D-region (Milan et al., 1999). Additionally, for January 21, 2005 there is SEP-induced ionization that started with the extremely strong GLE the previous day (Bieber et al., 2005). This SEP ionization may serve to decrease radar backscatter even more than just the substorm alone. It is possible that SuperDARN functioned more like a giant riometer than as a radar during this time period. With little backscatter, SuperDARN CPCP calculations become more heavily based on statistical modeling (which is strongly controlled by the IMF field) than current observational data. The same D-region conductivity enhancement can also cause screening above each MINIS balloon, making direct comparisons between conjugate points even more difficult.

With poor agreement between SuperDARN CPCP and MINIS horizontal electric fields, we cannot add much confidence to extrapolating the MINIS electric field and particle precipitation observations into the northern hemisphere. This lack of agreement does not mean future connections between the two polar cap regions are impossible. Rather, we assert that any such extrapolation must be made cautiously.

5. Conclusion

During the January 21, 2005 as an interplanetary shock arrived at earth, the MINIS balloon campaign had two payloads aloft in the stratosphere near Antarctica with X-ray detectors and dc-electric field probes. Although the MINIS-observed REP events coincide with magnetospheric compression when the impulses arrived, neither payload measured direct electric field impulses. We observe that the electric field enhancements are consistent with typical substorm growth and sunward plasma convection in the magnetosphere. Near the sec-

ond impulse arrival, we suggest that ionospheric conductivity enhancements weaken the observed electric field in both the poleward and eastward components. Finally, there is generally poor coincidental agreement between northern hemisphere peak CPCP measured by SuperDARN and maxima in electric fields measured by MINIS 2S and 3S in the southern hemisphere. This makes extrapolation of MINIS observations into the northern hemisphere much more difficult to make. Poor agreement between SuperDARN and MINIS suggests one or more of the following. There could be a real lack of conjugacy in the electric field between measurements sites in the northern and southern polar caps. We may not be making a valid comparison between the local (balloon) horizontal electric field and larger scale (radar) convection maps. Lastly, precipitation-induced density enhancements in the D-region ionosphere could absorb the HF radar signal and make the convection map output more reliant on statistical modeling and based less on physical backscatter returns. This same precipitation could also cause D-region screening at the balloons as well, making evidence of conjugacy more difficult to extract.

Acknowledgments

We thank our South African support, which included many people from both SANAP and DEAT. We also thank the folks at CSBF for help in test launching from McMurdo in 2003. Thanks to Dr. F. Mozer for providing Cluster data, Dr. Petrinec for providing a useful visualization tool of the shock impingement on the magnetopause, and Dr. Greenwald for helpful discussions regarding SuperDARN. We also thank our reviewers for their insightful comments. This work was supported under NSF Grants ATM-0233370 and OPP-0230441.

References

Araki, T., Fujitani, S., Emoto, M., et al. Anomalous sudden commencement on March 24, 1994. J. Geophys. Res. Space Phys. 102, 14075–14086, 1997.

Bering, E.A., Benbrook, J.R. Conjugate ionospheric electric-field measurements. Ann. Geophys. A. Upper Atmos. Space Sci. 5, 485–502, 1987.

Bering, E.A., Benbrook, J.R., Haacke, R., et al. The intense magnetic storm of December 19, 1980 – Observations at $L = 4$. J. Geophys. Res. Space Phys. 96, 5597–5617, 1991.

Bieber, J.W., Clem, J., Evenson, P. et al. Largest GLE in half a century: neutron monitor observations of January 20, 2005 Event. 29th International Cosmic Ray Conference, Pune, 1, 237–240, 2005.

Blake, J.B., Gussenhoven, M.S., Mullen, E.G., et al. Identification of an unexpected space radiation hazard. IEEE Trans. Nucl. Sci. 39, 1761–1764, 1992.

Clilverd, M.A., Rodger, C.J., Millan, R.M., et al. Energetic particle precipitation into the middle atmosphere triggered by a coronal mass ejection. J. Geophys. Res. Space Phys., 112, 2007.

Coumans, V., Gerard, J.C., Hubert, B., et al. Morphology and seasonal variations of global auroral proton precipitation observed by IMAGE-FUV. J. Geophys. Res. Space Phys., 109, 2004.

De la Beaujardiere, O., Vondrak, R., Heelis, R., et al. Auroral arc electrodynamic parameters measured by Ae–C and the Chatanika radar. J. Geophys. Res. Space Phys. 86, 4671–4685, 1981.

Dungey, J.W. Interplanetary magnetic field and auroral zones. Phys. Rev. Lett. 6, 47–48, 1961.

Elkington, S.R., Hudson, M.K., Wiltberger, M.J., et al. MHD/particle simulations of radiation belt dynamics. J. Atmos. Sol. Terr. Phys. 64, 607–615, 2002.

Foat, J.E., Lin, R.P., Smith, D.M., et al. First detection of a terrestrial MeV X-ray burst. Geophys. Res. Lett. 25, 4109–4112, 1998.

Gauld, J.K., Yeoman, T.K., Davies, J.A., et al. SuperDARN radar HF propagation and absorption response to the substorm expansion phase. Ann. Geophys. 20, 1631–1645, 2002.

Gosling, J.T., Bame, S.J., McComas, D.J., et al. Coronal mass ejections and large geomagnetic storms. Geophys. Res. Lett. 17, 901–904, 1990.

Holzworth, R.H., Bering, E.A. Ionospheric electric fields from stratospheric balloon borne probes, in: Pfaff, R., Borovsky, J., Yong, D. (Eds.), Measurement Techniques for Space Plasmas, Fields. American Geophysical Union, Washington, DC, 1998.

Hudson, M.K., Elkington, S.R., Lyon, J.G., et al. Simulations of radiation belt formation during storm sudden commencements. J. Geophys. Res. Space Phys. 102, 14087–14102, 1997.

Hudson, M.K., Kotelnikov, A.D., Li, X., et al. Simulation of proton radiation belt formation during the March 24, 1991 SSC. Geophys. Res. Lett. 22, 291–294, 1995.

Kokorowski, M., Sample, J.G., Holzworth, R.H., et al. Rapid fluctuations of stratospheric electric field following a solar energetic particle event. Geophys. Res. Lett., 33, 2006.

Li, X.L., Roth, I., Temerin, M., et al. Simulation of the prompt energization and transport of radiation belt particles during the March 24, 1991 SSC. Geophys. Res. Lett. 20, 2423–2426, 1993.

Looper, M.D., Blake, J.B., Mewaldt, R.A., et al. Observations of the remnants of the ultrarelativistic electrons injected by the strong SSC Of 24 March 1991. Geophys. Res. Lett. 21, 2079–2082, 1994.

McPherron, R.L. Growth phase of magnetospheric substorms. J. Geophys. Res. 75, 5592–5599, 1970.

Milan, S.E., Davies, J.A., Lester, M. Coherent HF radar backscatter characteristics associated with auroral forms identified by incoherent radar techniques: a comparison of CUTLASS and EISCAT observations. J. Geophys. Res. Space Phys. 104, 22591–22604, 1999.

Millan, R.M., Lin, R.P., Smith, D.M., et al. X-ray observations of MeV electron precipitation with a balloon-borne germanium spectrometer. Geophys. Res. Lett., 29, 2002.

Mozer, F.S., Bogott, F.H., Tsurutani, B. Relations between ionospheric electric-fields and energetic trapped and precipitating electrons. J. Geophys. Res. 78, 630–639, 1973.

Mozer, F.S., Serlin, R. Magnetospheric electric field measurements with balloons. J. Geophys. Res. 74, 4739–4754, 1969.

Mullen, E.G., Gussenhoven, M.S., Ray, K., et al. A double-peaked inner radiation belt – cause and effect as seen on CRRES. IEEE Trans. Nucl. Sci. 38, 1713–1717, 1991.

Petrinec, S.M., Russell, C.T. Near-Earth magnetotail shape and size as determined from the magnetopause flaring angle. J. Geophys. Res. Space Phys. 101, 137–152, 1996.

Ruohoniemi, J.M., Baker, K.B. Large-scale imaging of high-latitude convection with super dual auroral radar network HF radar observations. J. Geophys. Res. Space Phys. 103, 20797–20811, 1998.

Sample, J.G., Kokorowski, M., McCarthy, M.P. et al. First simultaneous observations of MeV electron precipitation from multiple balloon-borne spectrometers. Geophys. Res. Lett., submitted for publication.

Seppälä, A., Verronen, P.T., Kyrola, E., et al. Solar proton events of October–November 2003: ozone depletion in the northern hemisphere polar winter as seen by GOMOS/Envisat. Geophys. Res. Lett., 31, 2004.

Shue, J.H., Chao, J.K., Fu, H.C., et al. A new functional form to study the solar wind control of the magnetopause size and shape. J. Geophys. Res. Space Phys. 102, 9497–9511, 1997.

Shue, J.H., Song, P., Russell, C.T., et al. Magnetopause location under extreme solar wind conditions. J. Geophys. Res. Space Phys. 103, 17691–17700, 1998.

Vampola, A.L., Korth, A. Electron-drift echoes in the inner magnetosphere. Geophys. Res. Lett. 19, 625–628, 1992.

Wygant, J., Mozer, F., Temerin, M., et al. Large-amplitude electric and magnetic-field signatures in the inner magnetosphere during injection of 15 MeV electron-drift echoes. Geophys. Res. Lett. 21, 1739–1742, 1994.

Yeoman, T.K., Lester, M., Cowley, S.W.H., et al. Simultaneous observations of the cusp in optical, DMSP and HF radar data. Geophys. Res. Lett. 24, 2251–2254, 1997.